Cortical Magnification in Human Visual Cortex Parallels Task Performance around the Visual Field

Noah C. Benson[1,2,3,*],
Eline R. Kupers[1,2,4], Antoine Barbot[1,2,5],
Marisa Carrasco[1,2,†], Jonathan Winawer[1,2,†]

Key Words

cortical magnification • primary visual cortex • retinotopic maps
fMRI • visual performance asymmetries

---

[1] Dept. of Psychology, New York University, New York, NY 10003

[2] Center for Neural Sciences, New York University, New York, NY 10003

[3] Current affiliation: eScience Institute, University of Washington, Seattle, WA 98122

[4] Current affiliation: Dept. of Psychology, Stanford University, Stanford, CA 94305

[5] Current affiliation: Spinoza Centre for Neuroimaging, Amsterdam, Netherlands

[†] Equal contributors.

[*] To whom correspondence should be addressed. Email: nben@uw.edu

Abstract

Human vision has striking radial asymmetries, with performance on many tasks varying sharply with stimulus polar angle. Performance is generally better on the horizontal than vertical meridian, and on the lower than upper vertical meridian, and these asymmetries decrease gradually with deviation from the vertical meridian. Here we report cortical magnification at a fine angular resolution around the visual field. This precision enables comparisons between cortical magnification and behavior, between cortical magnification and retinal cell densities, and between cortical magnification in twin pairs. We show that cortical magnification in human primary visual cortex, measured in 181 subjects, varies substantially around the visual field, with a pattern similar to behavior. We find that these radial asymmetries in cortex are larger than those found in the retina, and that they are correlated between monozygotic twin pairs. These novel findings indicate a tight link between cortical topography and behavior, and suggest that visual field asymmetries are, at least in part, heritable.

Significance Statement

Human vision depends on location. Performance on visual tasks declines precipitously with distance from the center of gaze. It is also highly asymmetric around the visual field: Performance is better on the horizontal than vertical meridian, and better on the lower than upper vertical meridian. We investigated the neurobiological basis of these performance asymmetries by comparing how several factors vary around the visual field: task performance, surface area in visual cortex, and retinal cell density. We find that asymmetries in the primary visual cortex map (1) closely parallel asymmetries in behavior, (2) are larger than asymmetries in retinal cell density, and (3) are correlated between twins. These findings advance our understanding of how visual system architecture shapes perception.

Introduction

The human visual system processes the visual world with an extraordinary degree of non-uniformity. At the center of gaze, we see fine details whereas in the periphery acuity is about 50 times lower (1). This eccentricity effect is mediated by a far greater density of photoreceptors and retinal ganglion cells (RGCs) for the fovea than periphery, as well as by a correspondingly greater amount of cortical surface area per degree of visual field (2).

Importantly, visual performance varies not only across eccentricity, but also as a function of polar angle (**Fig. 1**); at matched eccentricity, performance is better along the horizontal than the vertical meridian (horizontal-vertical asymmetry, or "anisotropy"; HVA) and better along the lower than the upper vertical meridian (vertical meridian asymmetry; VMA) (3-11). These asymmetries are present in several basic perceptual dimensions, including contrast sensitivity (3, 4, 6-8, 11-16) and spatial resolution (5, 10, 17-21).

Variations in performance around the visual field are substantial: they can be as pronounced as that of doubling the stimulus eccentricity (11, 20). Moreover, these asymmetries are in retinal coordinates: the shape of the performance fields are constant in head-centered (but not screen-centered) coordinates whether subjects are tested with their heads tilted or straight (6). This result suggests that the effects likely arise relatively early in the visual processing stream. Consistent with this interpretation, radial asymmetries vary with several low-level stimulus properties: Both the HVA and the VMA become more pronounced as target eccentricity, target spatial frequency, or number of distractors increase (3, 4, 8). These radial asymmetries are *not* general

hemifield or quarterfield effects; they are largest at the cardinal meridians, and decrease gradually as the angular distance from the vertical meridian increases (4, 7, 8, 10). Indeed, performance in many tasks is similar across all visual quadrants at 45° intercardinal locations (3, 4, 6, 7).

The causes of radial asymmetries in performance are largely unknown. A computational observer model shows that optical quality and cone density can only account for a small fraction of the performance differences with polar angle (22). Substantial additional radial asymmetries must therefore arise in downstream

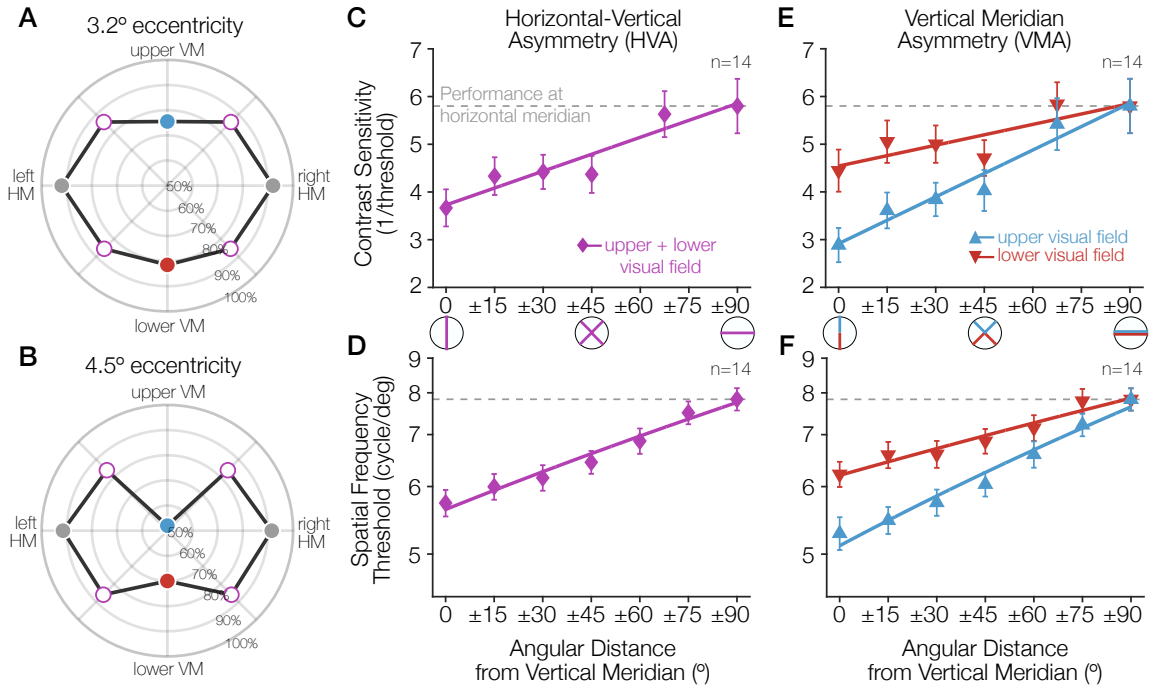

Figure 1. Task performance around the visual field. (A,B) Performance for a Gabor-orientation discrimination task is shown in polar coordinates. The plotted angle indicates the polar angle of the tested stimulus location, and the distance from the origin indicates the performance (percent correct) at that polar angle. The origin indicates chance performance. Gabor patches were presented at either (A) 3.2° or (B) 4.5° of eccentricity, with a spatial frequency of 10 and 12 cycles/degree, respectively. The HVA and VMA are evident in both plots and the asymmetries are more pronounced at the farther eccentricity (3) **(C-E)** As the angular distance from the vertical meridian increases, averaged across upper and lower, performance gradually improves, approaching the performance level at the horizontal (**C,D**), and the difference in performance between the upper and lower hemifields reduces (**E,F**). These gradual changes around the visual field have been observed for contrast sensitivity (7) (**C,E**; at 6° eccentricity) and acuity limit (10) (**D,F**; at 10° eccentricity). Each data point corresponds to the average contrast sensitivity (or spatial frequency threshold) at a given angular location, with ±1 S.E.M across observers. Spatial frequency was measured as the point at which orientation discrimination performance dropped to half-way between ceiling and chance performance. *Adapted from Carrasco et al. (2001) (3), Abrams et al. (2012) (7), and Barbot et al. (2020) (10).*

processing. Here we investigate whether (1) retinotopic maps in human V1 show stark radial asymmetries in cortical surface area; (2) these asymmetries are larger than those found in the retina; (3) these asymmetries fall off gradually with distance from the cardinal meridians, similar to human behavior; and (4) these asymmetries are correlated between monozygotic (MZ) twins, dizygotic (DZ) twins, and unrelated pairs. Such results would indicate a tight link between cortical topography, behavior and genetics.

Results

Polar asymmetries in cortical surface area. To examine polar angle asymmetries in the cortical representation, we used the largest human retinotopy dataset: the Human Connectome Project (HCP) 7 Tesla Retinotopy Dataset (*n*=181) (23). We calculated the surface area of a series of regions of interest (ROIs) defined by their visual field preference. Each ROI was centered on one of the four cardinal meridians. For each meridian, we defined several ROIs covering a gradually-increasing span of polar angle from ±10° to ±50° (**Fig. 2A**).

Analysis of these ROIs indicates that the cortical surface area in V1 is distributed asymmetrically, with remarkably large differences between the horizontal and vertical meridians. For example, within ±10° of the meridians, the surface area is ~50% greater for the horizontal than the vertical representation (**Figs. 2B, 2D**), and for the lower than the upper meridian (**Figs. 2C, 2E**). Within these ±10° ROIs, 160 of the 181 subjects have positive HVAs, and 155 have positive VMAs. The asymmetries are largest for narrow wedge ROIs. They decrease gradually with angular distance from the vertical meridian, with the VMA decreasing more sharply with distance than the HVA. Previous estimates of V1 cortical magnification by Horton and Hoyt (1991) (24) fall about halfway

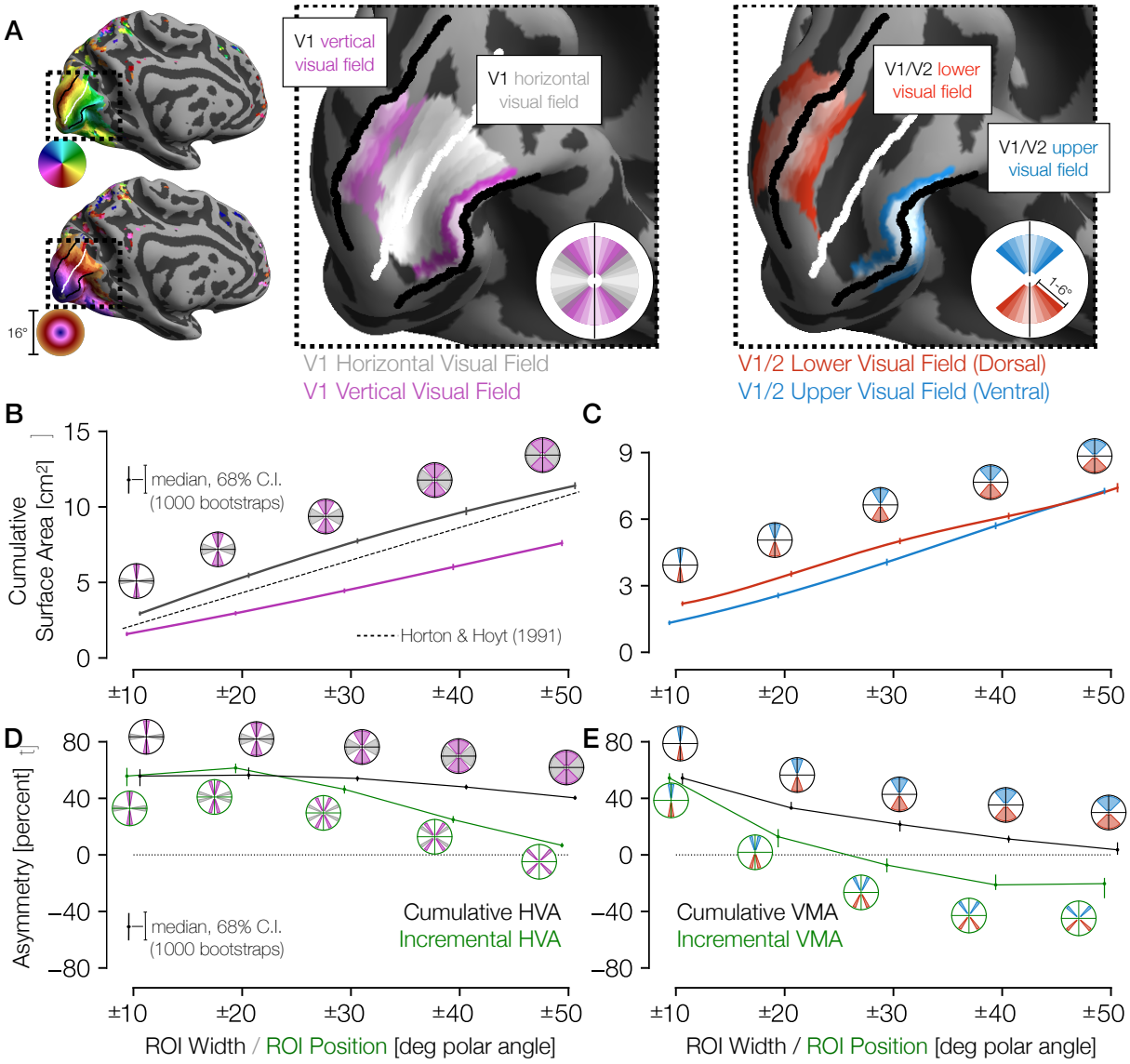

Figure 2. Cortical surface areas around the visual field. (A) Polar angle (top left) and eccentricity (bottom left) maps for example HCP subject 177746. The V1/V2 boundaries and the V1 horizontal meridian obtained via Bayesian inference are shown as black and white lines, respectively. The middle panel of A shows ROIs drawn with gradually increasing polar angle widths centered around the horizontal meridian (gray) and the vertical meridian (V1/V2 boundary; magenta), limited to 1-6° of eccentricity in V1 only. The right panel shows ROIs around the upper vertical meridian (ventral V1/V2 boundary; blue) and the lower vertical meridian (dorsal V1/V2 boundary; red) that include both V1 and V2. In this hemisphere, cortical surface area is greater near the horizontal than the vertical meridian and near the lower than the upper vertical meridian. **(B)** Surface area for increasingly large ROIs centered on the vertical (magenta) or horizontal (gray) meridian. The error bars indicate the 68% C.I. from bootstrapping. The circular icons show the visual field representations of the ROIs for the nearby data points. The *x*-values of data-points were slightly offset in order to facilitate visualization. The black dotted line shows the equivalent V1 ROI surface area as predicted by Horton and Hoyt (1991) (22). **(C)** Same as B, but for upper (blue) and lower (red) vertical meridians. **(D,E)** The surface areas are transformed to percent asymmetry, both for the cumulative ROIs (black) and incremental ROIs (green). Whereas cumulative ROIs represent a wedge of the visual field within a certain polar angle distance $\pm\theta$ of a cardinal axis, incremental ROIs represent dual 10°-wide wedges in the visual field a certain polar angle distance $\pm\theta$ *from* a cardinal axis. The percent asymmetry of *x* to *y* is defined as $100 \times (x-y)/\text{mean}(x, y)$. Positive values indicate greater area for horizontal than vertical (**D**) or for lower than upper regions (**E**).

between our measures for the vertical and horizontal meridians as they did not account for angular variation (see Methods).

Match between cortical and behavioral asymmetries. The cortical patterns we observe match behavioral asymmetries (**Fig. 1**), which also decrease gradually away from the vertical meridian, indicating a close correspondence between psychophysical performance and cortical representations in early visual retinotopic maps. One exception is a modest negative incremental VMA at inter-cardinal angles in cortex (**Fig. 2E**) not typically found in psychophysics. Overall, both behavior and surface area fall off gradually and are highly correlated (**Fig. 3**; Pearson's r = 0.96). We note that the behavioral pattern may vary with task, and so this correlation might differ for other tasks.

Asymmetries in cortical surface area by twin status and gender. The strong correlation between behavior and cortical surface area was computed at the group level, given that the two measures come from different groups. Nonetheless, there are individual differences in both the behavioral (11) and cortical surface area (23) measures. Because the cortical surface area measures come from the HCP dataset,

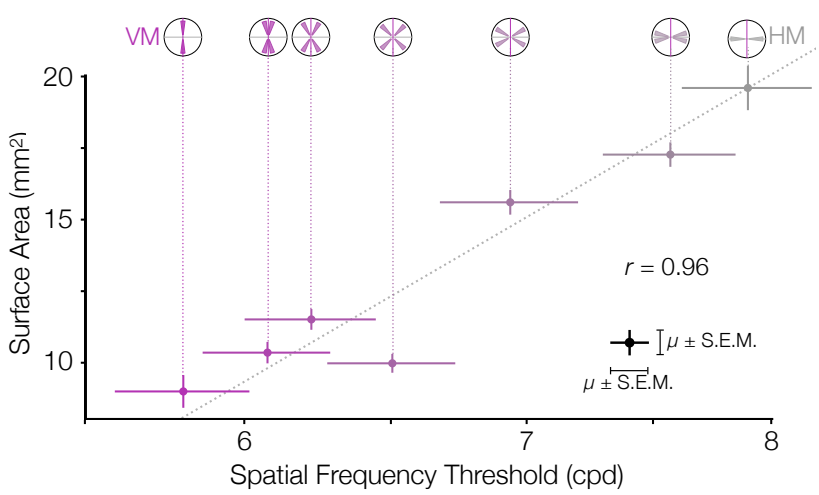

Figure 3. Asymmetries in behavior and cortical surface area are correlated. V1 surface area measured from the HCP (21) is highly correlated with the spatial frequency thresholds measured by Barbot *et al.* (2020) (10) in matched ROIs. Surface areas (y-axis) were computed for ROIs whose visual field positions were limited to 4-5° of eccentricity in order to match the psychophysical experiments. Areas were summed over regions indicated by the visual field insets (and divided by 2 for all ROIs except the VM and HM, since the latter two ROIs have half the visual field area of the other ROIs). The Pearson correlation is 0.96.

which include a large number of twin pairs, we were able to ask whether individual measures in surface area asymmetries (HVA and VMA) were shared between twin pairs. Indeed, for monozygotic twin pairs, the correlation of ROI surface area is about 40% for most ROIs (**Fig. 4**). This is substantially higher than the correlations for age-matched unrelated pairs, which are much closer to 0% for all ROIs. The correlations for dizygotic twins are numerically intermediate between monozygotic twins and unrelated pairs for both the HVA and the VMA. The number of twins is not large enough to make a precise estimate of a heritability fraction, as the heritability confidence combines the uncertainty in the MZ and the DZ data. The general pattern, however, whereby the largest correlation is for MZ twins and the smallest is for unrelated pairs, is clearly consistent with the radial asymmetries having a heritable component. Note that the correlations of the HVA between unrelated pairs is non-zero because females have, on average, a marginally higher HVA than males across cumulative wedges (**Fig. S1,** bottom row) and because the unrelated pairs used in the calculations excluded subject pairs that were not age- and gender-matched in order to better resemble the sets of

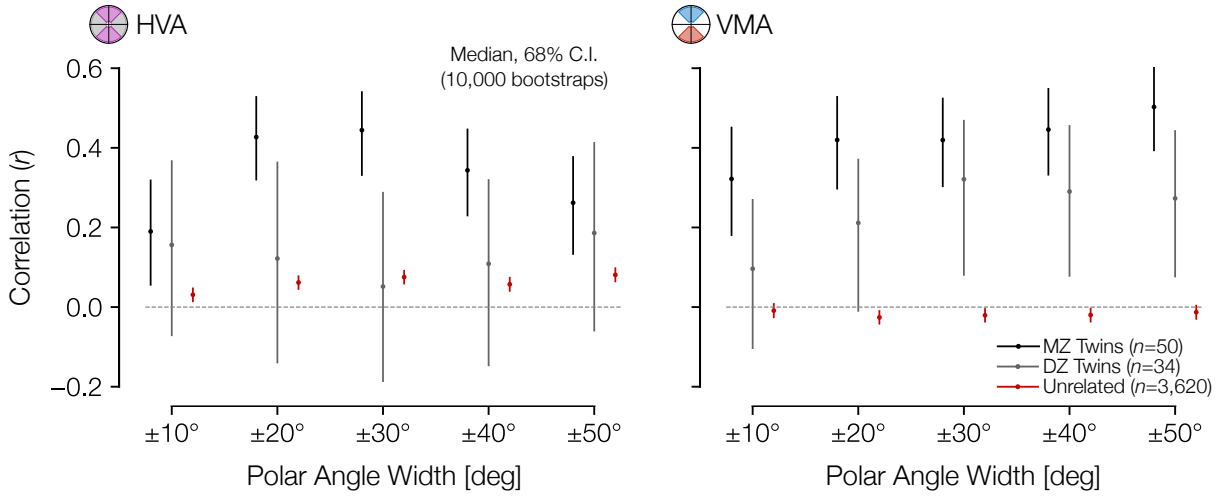

Figure 4. Asymmetries in cortical surface area are correlated across twins. Intraclass correlation coefficient between twin pairs (MZ and DZ) and age- and gender-matched unrelated pairs. The correlations were computed for the HVA (left) and (VMA) right for different size wedges, as in **Figure 2**.

twin pairs. If pairs that are not gender-matched are included, the HVA correlations between unrelated pairs become statistically indistinct from zero.

Because cortical surface area differs between males and females, we examined whether the radial asymmetries do as well. We find that the cortical VMA and HVA do not differ substantially by sex or across age-groups (**Fig. S1**. This is consistent with psychophysical findings that the HVA and VMA are similar in males and females (10, 16). Whereas the average size of V1 is about 10% larger in males, V1 size normalized to the entire cortical surface area is similar for males and females (**Fig. S2**).

Asymmetries in cortical surface area and retinal cell density. Asymmetries around the visual field exist in many parts of the visual system, beginning with the optics and the retinal cone density. However, the cortical asymmetries are not simply inherited from the photoreceptors. Rather, the asymmetries become larger in measures of retinal ganglion cell (RGC) density compared to cones, and become substantially larger still in

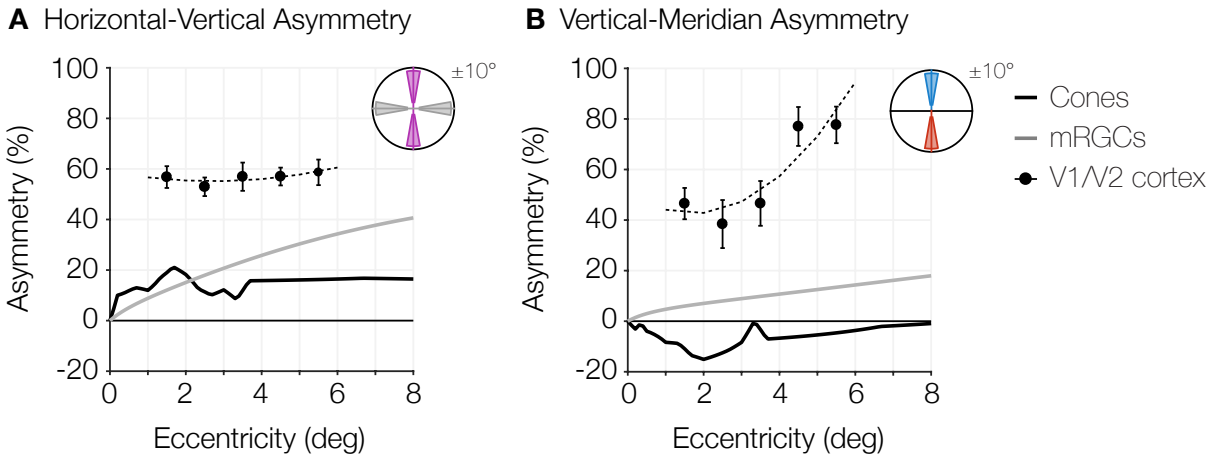

Figure 5. Asymmetries from retina and visual cortex. (**A**) HVA and (**B**) VMA for cone density (black line) and mRGC density (grey line) when comparing the cardinal meridians, and V1/V2 cortical surface area within the ±10° ROIs (black markers) as a function of eccentricity. Cone density data are in counts/deg^2 (23). Midget RGC densities represent the receptive field counts/deg^2 using the quantitative model by Watson (2014) (24). V1/V2 cortex data are calculated from the cortical surface area in mm^2/deg^2 within 1° non-overlapping eccentricity bands from 1-6° of the ±10° ROIs. Markers and error bars represent the median and standard deviation across bootstraps, respectively. Data are fitted with a 2nd-degree polynomial. Goodness of fit are R^2_{HVA} = 0.57 and R^2_{VMA} = 0.81.

surface area of V1 (**Fig. 5**). Below 8° of eccentricity, cone density is greater on the horizontal than vertical meridian, with an HVA of ~20% (**Fig. 5A**) (25). Over the same eccentricity range, the HVA measures up to 40% in midget RGC density and 60% in visual cortex. In this eccentricity range, the VMA is slightly negative for cone density (**Fig. 5B**): the upper visual field (inferior retina) has higher cone density than the lower visual field (superior retina), indicating that cone density cannot be the source of the behavioral VMA (22). The VMA becomes positive in midget RGC density (up to ~20%) and larger still in the cortex (~40-80%). Hence, the radial asymmetries are substantially amplified in cortex compared to both the photoreceptors and the mRGCs.

This finding that polar angle asymmetries are amplified in successive stages of visual processing parallels findings regarding eccentricity: The cone density is greatest in the fovea, falling off with increasing eccentricity (25); this fall-off with eccentricity becomes steeper in the midget ganglion cell array (26), and steeper still in V1 (27). This means that the eccentricity gradient becomes steeper in successive processing stages. Given that most human visual perception relies on signals passing through V1, the further amplification of both the foveal bias and the radial asymmetries (HVA and VMA) likely have important implications for visual performance. The overall size of V1 and the cortical magnification function (averaged across polar angles) correlate with various measures of perception, including vernier acuity (28, 29) and the strength of some illusions (30). The cortical HVA and VMA in individuals may similarly predict radial asymmetries in their visual performance.

Discussion

Here, we reported cortical magnification at a fine angular resolution around the visual field and in the largest available subject pool, allowing us to measure the organization of cortical magnification with high precision. This precision in turn enabled our comparison between cortical magnification and behavior, between cortical magnification of twins, and between cortical magnification and retinal cell densities. The fine angular resolution is especially important for assessing the VMA. The VMA falls off sharply with distance from the vertical meridian: the size of the VMA within 10° of the vertical meridian is ~50%, whereas within 40° it is only ~10%. Prior studies have also shown radial asymmetries in visual cortex, in fMRI BOLD amplitude (31), in cortical magnification in human (32) and monkey (33), in population receptive field size (32), and in spatial frequency preference in human (34). For instance, Silva *et al*. (32) quantified cortical magnification in visual field quadrants (lower, upper, left, and right) for V1-V3. Comparing the surface areas of these quadrants, the authors report a greater magnification in the horizontal than the vertical quadrants and in the lower than the upper quadrant. This report agrees broadly with our measurements. However, neither behavior (3, 4, 7, 8, 10) nor cortical magnification is uniform within quadrants (**Fig. 2**). Hence assessing the relationship between cortical area and behavior requires measurement at a fine angular resolution.

Although variation in performance with respect to polar angle is less well studied than variation with respect to eccentricity, the size of the polar angle asymmetries in behavior is substantial. At 6° of eccentricity, the VMA and HVA in contrast sensitivity are >40% (**Figs. 1C**, 0° v. dotted-line; **1E**, upper v. lower at 0°). Additionally, the shapes

of these performance fields are resilient. For example, both the HVA and VMA are present for stimuli of different orientation, size, luminance, eccentricity, and spatial frequency (3-11). They also remain constant after both endogenous (voluntary) (16) and exogenous (involuntary) (3, 4) covert attention have exerted their effects on perception. That is, attention improves performance in a variety of tasks at all polar angles to a similar degree, *e.g.*, orientation discrimination and acuity, but does not diminish the radial asymmetries. Furthermore, the shape of performance fields is maintained in visual short-term memory (VSTM), implying that the quality with which a visual stimulus is perceived and encoded at different locations affects the quality with which it is maintained in VSTM (5). The results reported here–differential resources devoted to the different meridians in V1–may underlie both the perceptual and VSTM phenomena.

To conclude, this study reveals a tight link between human perception around the visual field and the anatomical organization of V1: both cortical magnification and visual task performance are greatest on the horizontal meridian, lesser on the lower vertical meridian, and the lowest on the upper vertical meridian. Both the behavioral and cortical HVA/VMA fall off gradually with angular distance from the cardinal meridians, with both performance and magnification reaching equality at the inter-cardinal angles. Moreover, we show that these cortical asymmetries reflect the large-scale organization of the visual pathways, becoming more stark at multiple successive stages, and that they are correlated between twin pairs. These findings show a clear relation between biological structure and behavior and reveal how an increasingly large radial asymmetry across the visual system contributes to visual perception. Comprehensive models of vision must take into account not only performance and

anatomical variations across eccentricity, but also variations as a function of polar angle across iso-eccentric locations.

Methods

Code and Data Availability. All data analyzed in this project was previously available from other sources. The results of all analyses and the source code required to produce them, as well as documentation, are publicly available at an Open Science Framework website (**https://osf.io/5gprz/**; DOI:10.17605/OSF.IO/5GPRZ). This paper's Github repository can be found at **https://github.com/noahbenson/performance-fields/**.

Data Sources. Structural preprocessed data were obtained from the Human Connectome Project Young Adult dataset (HCP; https://db.humanconnectome.org/) (35). Genotype data for these subjects (*i.e.*, twin pairings) were also obtained from the HCP. Retinotopic maps were obtained from the HCP 7 Tesla Retinotopy Dataset (23). Behavioral data were obtained from Abrams *et al.* (2012) (7) and Barbot *et al.* (2020) (10). Behavioral data were obtained from a separate set of subjects than the structural and retinotopic mapping data because we have no access the HCP subjects to administer behavioral experiments. The HCP includes some simple acuity measurements for the subjects, but these measures are not positioned around the visual field.

Cortical Calculations. We used the Human Connectome Project (HCP) 7 Tesla retinotopy dataset (23) (n = 181 subjects) to characterize the cortical HVA and VMA. We computed the percent difference in cortical surface area for V1 (HVA) or V1/V2 (VMA)

using the formula $\Delta(x_{V1}, x_{V2}) = 100 \times (x_{V1} - x_{V2}) / \text{mean}(x_{V1}, x_{V2})$. We did this by first defining regions of interest (ROIs) near the cardinal meridians (upper vs lower: VMA; horizontal vs vertical: HVA). The reason for using V1/V2 for the VMA is that the vertical meridian is represented on the border of V1/V2 and the polar angle retinotopy data often do not reach the vertical meridian. Rather than making the analyses contingent on finding the exact border between V1 and V2, we instead analyzed regions spanning both V1 and V2, which were unambiguous to define. This is because the 80º line or the 70º line, for example, could be easily identified on both sides of the V1/V2 boundary. To test the angular specificity of these asymmetries, we defined several wedge-shaped ROIs surrounding each cardinal meridian, ranging in width from narrow to wide (±10° to ±50° of polar angle from the meridians). All ROIs were restricted to 1-6º of eccentricity.

ROIs were computed in several steps. First, to automatically label V1 and V2 and to deduce smooth polar angle and eccentricity maps, we performed Bayesian inference on each hemisphere using the measured retinotopic maps from the HCP retinotopy dataset as the Bayesian observation (36). This process yields a set of "inferred" retinotopic maps for each subject whose smoothness makes them ideal for drawing ROI boundaries. However, because it is possible that this automated algorithm produces small errors in localizing the precise boundaries of V1 and V2, we have taken additional steps to minimize the impact of such errors. To find the ROIs about a particular meridian (horizontal, upper vertical, or lower vertical) for a polar angle width of θ (i.e., $\theta \in \{10°, 20°, 30°, 40°, 50°\}$), V1 and V2 ROIs were divided into 5 strips based on the inferred eccentricity (1-2°, 2-3°, 3-4°, 4-5°, 5-6°). Within each of these strips and on each side of the relevant meridian, we calculated the mean distance along the

cortex required to cross $\theta°$ of polar angle from the meridian. The vertices within the eccentricity strip and within this distance were included in the appropriate ROI. ROIs found for all eccentricity strips were joined to form the overall ROI with width α. For the ROIs used in the HVA comparison, the V2 sections of the vertical meridian ROIs were excluded in order to compare the V1 horizontal to only the V1 vertical; accordingly, these ROIs may be slightly less precise than the VMA ROIs. Example ROIs are shown in **Figure 2A**. A separate set of wedges and eccentricities was used for the data in **Figure 3** that was matched to the behavioral experiment. The polar angle strips used to infer the surface area for this figure were $\theta_{3C} \in \{7.5°, 22.5°, 37.5°, 45°\}$ and the eccentricity bands were 4-4.5°, and 4.5-5°. The surface areas of these cumulative wedge ROIs were calculated then recombined via addition and subtraction into the surface areas of the set of seven 15°-wide ROIs centered at the VM, the HM, and the five non-overlapping 15°-wide strips between. Explicitly, these ROIs represent 0±7.5°, 15±7.5°, 30±7.5°, 45±7.5°, *etc*., all the way around the visual field.

In both the 10°- and the 15°-wide strips, the HVA surface areas of each ROI, which were calculated from V1 alone, were checked against the areal cortical magnification formula of V1 described by Horton and Hoyt (1991) (24): $m_{HH}(x, y) = (17.3\text{mm} / (\rho(x, y) + 0.75°))^2$ where $\rho(x, y)$ is the eccentricity in degrees of the visual field coordinate (x, y). The integral of $m_{HH}(x, y)$ over the visual field representation of an ROI yields the cortical surface area c_{ROI} predicted by Horton and Hoyt for that ROI: $c_{ROI} = \int_{(x,y)\in ROI} m_{HH}(x,y)\, dx\, dy$. Because Horton and Hoyt's formula does not incorporate polar angle, its predictions should fall between the surface areas of the vertical ROIs and the horizontal ROIs. For both strip widths, this was the case. For the 10°-, 20°-, 30°-, 40°-,

and 50°-wide ROIs in **Figure 2B**, Horton and Hoyt predict 2.2, 4.3, 6.5, 8.6, and 10.8 cm^2 surface areas, respectively. For the 15°-wide strips, the predicted surface area for each strip is 12.8 mm^2, which is between the surface areas of the vertical and the horizontal ROIs in **Figure 3**.

Intraclass correlation (ICC) values plotted in **Figure 4** were calculated between the 50 monozygotic twins, the 34 dizygotic twins, and the 3,620 age- and sex-matched unrelated pairs from the HCP 7T retinotopy dataset (23). The 3,620 unrelated pairs represents the subset of the possible 16,290 unique subject pairs from the 181 retinotopy subjects that are not twins or otherwise related, that are the same gender, and that are in the same HCP age-group. Error bars are plotted as the 16th and 84th percentiles across bootstraps.

Retinal Calculations. The raw data used for **Figure 5** were previously published or from publicly available analysis toolboxes. Cone density data were extracted from post-mortem retinal tissue of 8 human retinae published by Curcio *et al.* (1990) (25) for 0-8° eccentricities (step size 0.1°) and summarized in the ISETBIO toolbox (https://github.com/isetbio/isetbio) (37). Midget retinal ganglion cell (mRGC) densities were extracted from the analytic model by Watson (2014) (26). Cortical asymmetries were computed from the HCP 7 Tesla retinotopy dataset (23) as percent difference in V1/V2 cortical surface area in ±10° wedges centered on the cardinal meridians for 1° bins between 1-6° eccentricity. Median and standard error of cortical surface area were computed from bootstrapped data across subjects (1000 iterations).

Meridian asymmetries in cone density and mRGC density were defined as percent change in density values at the cardinal meridians (for retina) or V1/V2 cortical surface area within polar angle wedges centered on cardinal meridians as follows:

$$\mathrm{HVA} = 100\frac{\mathrm{mean(nasal, temporal)} - \mathrm{mean(superior, inferior)}}{\mathrm{mean(nasal, temporal, superior, inferior)}}$$

$$\mathrm{VMA} = 100\frac{\mathrm{superior} - \mathrm{inferior}}{\mathrm{mean(superior, inferior)}}$$

Limitations. The calculations of cortical surface area were performed with state-of-the-art data (23) and methods (36), but some limitations on the accuracy of the measured values remains. First, the method used to detect the V1/V2 boundary is automated and can produce boundaries with slight errors. Our use of a distance-based threshold to find wedge-ROIs was explicitly chosen to mitigate such potential errors. Additionally, cortical surface distances were calculated using Dijkstra's graph-based algorithm (38). Although Dijkstra's method can calculate the precise graph-distance between two vertices, the graph-distance must follow a path along the edges of the triangle mesh. Thus the graph-distance is an approximation of the actual geodesic distance along the cortical surface and is never less than the geodesic distance.

Quantification and Statistical Analysis. This manuscript does not assess statistical significance. Confidence intervals (CIs) computed for **Figures 1** and **3** are the standard error of the mean. CIs for **Figures 2, 4** and **5** are the standard deviation of the median across bootstraps. CIs for **Figure 3B** are the 16th and 84th percentiles across bootstraps.

Acknowledgements

We thank Antonio Fernández, Michael Jigo, and Drs. Marc Himmelberg and Jan Kurzawski for helpful comments. This work was supported by NIH NEI RO1-EY027401 to MC and JW as well as a Data Science Environments project award from the Gordon and Betty Moore Foundation (Award #2013-10-29) and the Alfred P. Sloan Foundation (Award #3835) to the University of Washington eScience Institute.

Author Contributions

MC and JW conceived of the project. NB performed all cortical surface analyses (**Figs. 2-4, S1,** and **S2**). EK performed all retinal analyses (**Fig. 5**). AB performed analysis and created **Figure 1**. NB, JW, and MC wrote the paper with feedback from AB and EK.

References

1. L. Frisen, A. Glansholm, Optical and neural resolution in peripheral vision. *Invest Ophthalmol* **14**, 528-536 (1975).
2. R. W. Rodieck, *The first steps in seeing* (Sinauer Associates, Sunderland, Mass., 1998), pp. xi, 562 p.
3. M. Carrasco, C. P. Talgar, E. L. Cameron, Characterizing visual performance fields: effects of transient covert attention, spatial frequency, eccentricity, task and set size. *Spat Vis* **15**, 61-75 (2001).
4. E. L. Cameron, J. C. Tai, M. Carrasco, Covert attention affects the psychometric function of contrast sensitivity. *Vision Res* **42**, 949-967 (2002).
5. L. Montaser-Kouhsari, M. Carrasco, Perceptual asymmetries are preserved in short-term memory tasks. *Atten Percept Psychophys* **71**, 1782-1792 (2009).
6. J. E. Corbett, M. Carrasco, Visual performance fields: frames of reference. *PLoS One* **6**, e24470 (2011).
7. J. Abrams, A. Nizam, M. Carrasco, Isoeccentric locations are not equivalent: the extent of the vertical meridian asymmetry. *Vision Res* **52**, 70-78 (2012).
8. A. S. Baldwin, T. S. Meese, D. H. Baker, The attenuation surface for contrast sensitivity has the form of a witch's hat within the central visual field. *J Vis* **12** (2012).
9. J. A. Greenwood, M. Szinte, B. Sayim, P. Cavanagh, Variations in crowding, saccadic precision, and spatial localization reveal the shared topology of spatial vision. *Proc Natl Acad Sci U S A* **114**, E3573-E3582 (2017).

10. A. Barbot, S. Xue, M. Carrasco, Spatial frequency asymmetries around the visual field. *Journal of Vision* **In Press** (2020).
11. M. M. Himmelberg, J. Winawer, M. Carrasco, Stimulus-dependent contrast sensitivity asymmetries around the visual field. *J Vis* **20**, 18 (2020).
12. J. Rovamo, V. Virsu, An estimation and application of the human cortical magnification factor. *Exp Brain Res* **37**, 495-510 (1979).
13. J. S. Pointer, R. F. Hess, The contrast sensitivity gradient across the human visual field: with emphasis on the low spatial frequency range. *Vision Res* **29**, 1133-1151 (1989).
14. S. Fuller, R. Z. Rodriguez, M. Carrasco, Apparent contrast differs across the vertical meridian: visual and attentional factors. *J Vis* **8**, 16 11-16 (2008).
15. R. Rosen, L. Lundstrom, A. P. Venkataraman, S. Winter, P. Unsbo, Quick contrast sensitivity measurements in the periphery. *J Vis* **14**, 3 (2014).
16. S. Purokayastha, M. Roberts, M. Carrasco, Voluntary attention improves performance similarly around the visual field. http://dx.doi.org/10.31234/osf.io/6fkys.
17. R. S. Anderson, M. O. Wilkinson, L. N. Thibos, Psychophysical localization of the human visual streak. *Optom Vis Sci* **69**, 171-174 (1992).
18. M. Mackeben, Sustained focal attention and peripheral letter recognition. *Spat Vis* **12**, 51-72 (1999).
19. E. Altpeter, M. Mackeben, S. Trauzettel-Klosinski, The importance of sustained attention for patients with maculopathies. *Vision Res* **40**, 1539-1547 (2000).
20. C. P. Talgar, M. Carrasco, Vertical meridian asymmetry in spatial resolution: visual and attentional factors. *Psychon Bull Rev* **9**, 714-722 (2002).
21. M. O. Wilkinson, R. S. Anderson, A. Bradley, L. N. Thibos, Neural bandwidth of veridical perception across the visual field. *J Vis* **16**, 1 (2016).
22. E. R. Kupers, M. Carrasco, J. Winawer, Modeling visual performance differences 'around' the visual field: A computational observer approach. *PLoS Comput Biol* **15**, e1007063 (2019).
23. N. C. Benson *et al.*, The Human Connectome Project 7 Tesla retinotopy dataset: Description and population receptive field analysis. *J Vis* **18**, 23 (2018).
24. J. C. Horton, W. F. Hoyt, The representation of the visual field in human striate cortex. A revision of the classic Holmes map. *Arch Ophthalmol* **109**, 816-824 (1991).
25. C. A. Curcio, K. R. Sloan, R. E. Kalina, A. E. Hendrickson, Human photoreceptor topography. *J Comp Neurol* **292**, 497-523 (1990).
26. A. B. Watson, A formula for human retinal ganglion cell receptive field density as a function of visual field location. *J Vis* **14** (2014).
27. D. L. Adams, J. C. Horton, A precise retinotopic map of primate striate cortex generated from the representation of angioscotomas. *J Neurosci* **23**, 3771-3789 (2003).

28. R. O. Duncan, G. M. Boynton, Cortical magnification within human primary visual cortex correlates with acuity thresholds. *Neuron* **38**, 659-671 (2003).
29. C. Song, D. S. Schwarzkopf, R. Kanai, G. Rees, Neural population tuning links visual cortical anatomy to human visual perception. *Neuron* **85**, 641-656 (2015).
30. D. S. Schwarzkopf, C. Song, G. Rees, The surface area of human V1 predicts the subjective experience of object size. *Nat Neurosci* **14**, 28-30 (2011).
31. T. Liu, D. J. Heeger, M. Carrasco, Neural correlates of the visual vertical meridian asymmetry. *J Vis* **6**, 1294-1306 (2006).
32. M. F. Silva *et al.*, Radial asymmetries in population receptive field size and cortical magnification factor in early visual cortex. *Neuroimage* **167**, 41-52 (2018).
33. D. C. Van Essen, W. T. Newsome, J. H. Maunsell, The visual field representation in striate cortex of the macaque monkey: asymmetries, anisotropies, and individual variability. *Vision Res* **24**, 429-448 (1984).
34. S. Aghajari, L. N. Vinke, S. Ling, Population spatial frequency tuning in human early visual cortex. *J Neurophysiol* **123**, 773-785 (2020).
35. D. C. Van Essen *et al.*, The Human Connectome Project: a data acquisition perspective. *Neuroimage* **62**, 2222-2231 (2012).
36. N. C. Benson, J. Winawer, Bayesian analysis of retinotopic maps. *Elife* **7** (2018).
37. N. P. Cottaris, H. Jiang, X. Ding, B. A. Wandell, D. H. Brainard, A computational-observer model of spatial contrast sensitivity: Effects of wave-front-based optics, cone-mosaic structure, and inference engine. *J Vis* **19**, 8 (2019).
38. E. W. Dijkstra, A note on two problems in connexion with graphs. *Numerische Mathematik* **1**, 269-271 (1959).

Supplemental Materials

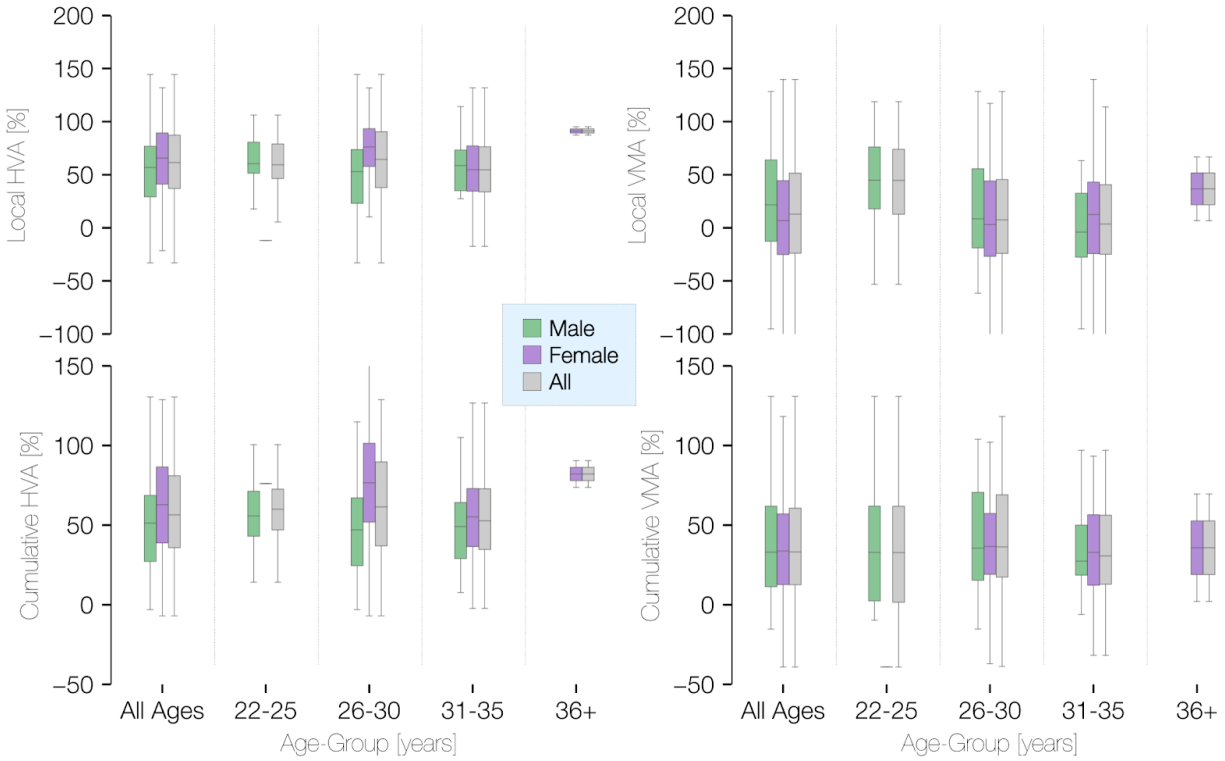

Supplemental Figure 1. Visual field asymmetry in terms of age and gender at ±20° of polar angle. Plots of the local (top row) and cumulative (bottom row) asymmetry across subjects in terms of age and gender. The percent horizontal-vertical asymmetry (HVA: horizontal ROI surface area minus vertical ROI surface area, divided by the mean surface area across horizontal and vertical ROIs) is shown in the left column, and the vertical meridian asymmetry (VMA: upper vertical ROI surface area minus lower vertical ROI surface area, divided by the mean surface area across upper and lower ROIs) is shown in the right column. Box-plots show the median (central horizontal line), quartiles (shaded box), and ±95% percentiles (lines). There is only 1 female subject in the 22-25 age-group and no males in the 36+ age-group.

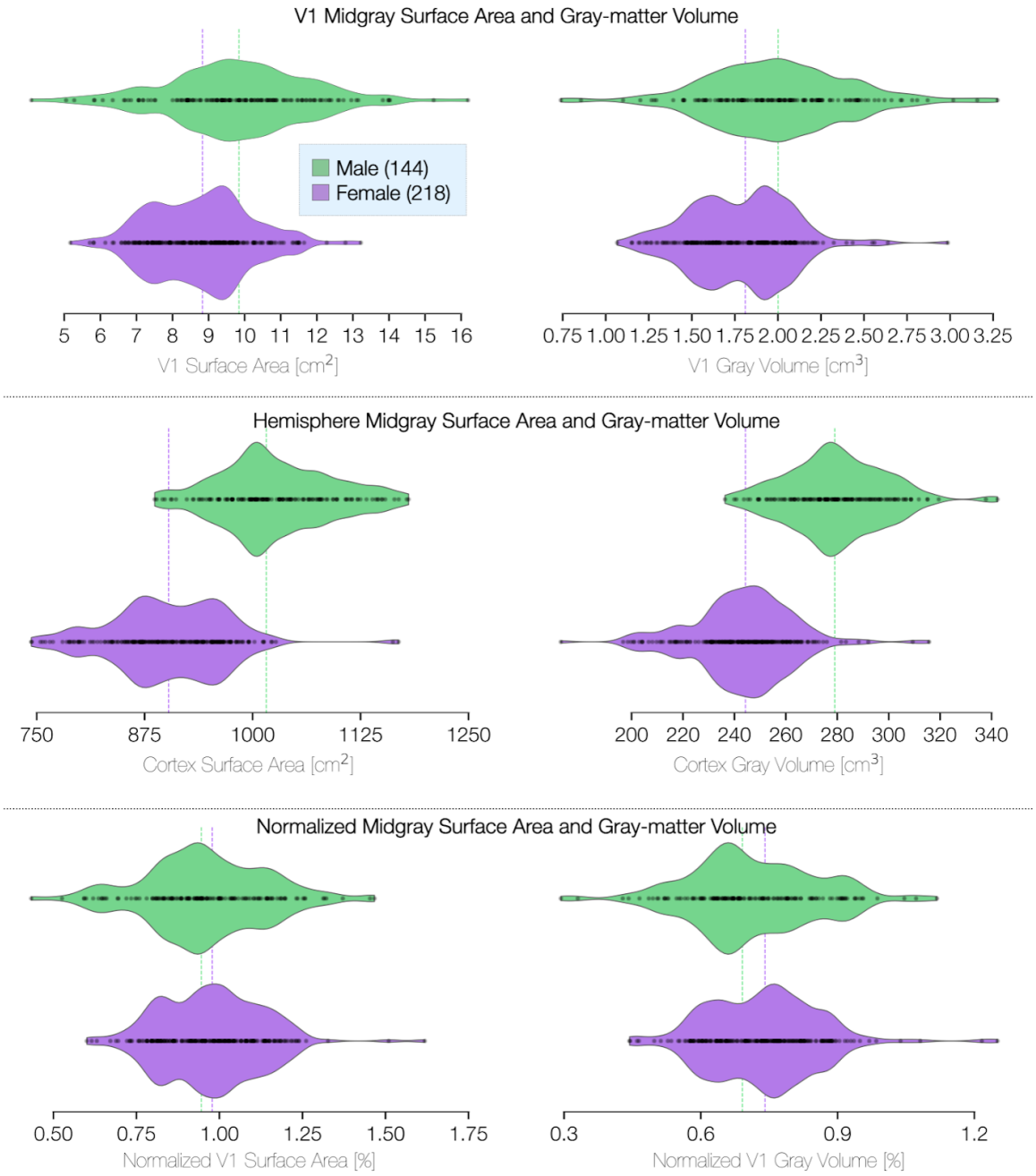

Supplemental Figure 2. V1 size and volume differences in terms of sex. ROI is limited to V1 between 1° and 6° of eccentricity. Violin plots terminate at the exact extrema of the dataset. Surface area was calculated on the mid-gray surface. Volume calculations include the entire gray-matter layer. Whole-hemisphere calculations for surface area and volume exclude the region corresponding to the corpus callosum.